



Synodic Period Channel Modeling and Coding Scheme for Deep Space Optical Communications


YAOSHENG ZHANG , Graduate Student Member, IEEE

JIAN JIAO , Senior Member, IEEE
Harbin Institute of Technology, Shenzhen, China
Peng Cheng Laboratory, Shenzhen, China

KE ZHANG , Member, IEEE

YE WANG , Member, IEEE
Peng Cheng Laboratory, Shenzhen, China

RONGXING LU , Fellow, IEEE
University of New Brunswick, Fredericton, NB, Canada

QINYU ZHANG , Senior Member, IEEE
Harbin Institute of Technology, Shenzhen, China
Peng Cheng Laboratory, Shenzhen, China

In this article, we design an end-to-end free-space optical (FSO) communication coding scheme for deep space exploration. Take the

Manuscript received 1 September 2023; revised 21 November 2023; accepted 6 January 2024. Date of publication 15 January 2024; date of current version 12 April 2024.

DOI. No. 10.1109/TAES.2024.3353726

Refereeing of this contribution was handled by J. Choi.

This work was supported in part by the National Natural Sciences Foundation of China (NSFC) under Grant 62071141, Grant 62027802, and Grant 61831008, in part by the Shenzhen Science and Technology Program under Grant JSGG20220831110801003 and Grant GXWD20231127123203001, and in part by the Major Key Project of PCL Department of Broadband Communication.

Authors' addresses: Yaosheng Zhang, Jian Jiao, and Qinyu Zhang are with the Guangdong Provincial Key Laboratory of Aerospace Communication and Networking Technology, Harbin Institute of Technology, Shenzhen 518055, China, and also with the Peng Cheng Laboratory, Shenzhen 518055, China, E-mail: (zhangyaoshg@foxmail.com; jiaojian@hit.edu.cn; zqy@hit.edu.cn); Ke Zhang and Ye Wang are with the Peng Cheng Laboratory, Shenzhen 518055, China, E-mail: (zhangk@pcl.ac.cn; wangy02@pcl.ac.cn); Rongxing Lu is with the Faculty of Computer Science, University of New Brunswick, Fredericton, NB E3B 5A3, Canada, E-mail: (rlu1@unb.ca). (*Corresponding authors: Jian Jiao; Ye Wang; Qinyu Zhang.*)

© 2024 The Authors. This work is licensed under a Creative Commons Attribution-NonCommercial-NoDerivatives 4.0 License. For more information, see <https://creativecommons.org/licenses/by-nc-nd/4.0/>

Mars exploration as an example, we first establish the synodic period FSO channel model by taking into account the solar scintillation, and derive the corresponding upper bound of bit error rate (BER) for L -ary pulse position modulation (LPPM). Then, we propose a staircase code-ordered statistics decoder (SC-OSD) algorithm for staircase low density parity check (LDPC) codes under synodic period FSO channel, and derive the probability density function (PDF) and Gaussian approximation of the ordered statistics of the SC-OSD algorithm, which provide a guideline to derive a lower bound of block error rate (BLER) and reduce the decoding complexity of SC-OSD. Furthermore, we propose a soft OSD-sliding window decoding (SOSD-SWD) algorithm for staircase LDPC codes under scintillation states to address the error floor problem in conventional SWD decoder. Simulation results validate that the proposed SOSD-SWD algorithm can achieve much lower BER than the related algorithms in all scintillation conditions, and shed light to tradeoff the achievable BER and complexities under different scintillation conditions.

I. INTRODUCTION

Deep space exploration has come a long way since the Lunar and Mars missions in the 1960s [1], which aim to uncover the mysteries of the universe, search for extraterrestrial life, and find inhabitable space over the past six decades. Deep space communication [2] serves as a crucial guarantee for deep space exploration, which is characterized by long distances, large propagation latency, and low signal-to-noise ratio (SNR). To meet the increasing demands of higher data rates under limited power resource, free-space optical (FSO) communication has become increasingly important in deep space exploration due to its advantages of large bandwidth, low power consumption, and small device size [3], [4], [5]. However, there are still essential challenges in deep space FSO communication for reliable transmission, such as channel modeling and an efficient coding scheme [6], [7].

In long-term planetary exploration missions, it is important to consider the uncertainty of the communication environment caused by the positional variation of the Earth and the planetary probe relative to the Sun in a synodic period. Deep space FSO channel modeling [8] is an essential step in optimizing the design of an end-to-end communication scheme. Ivanov et al. [9] investigate the deep space optical Poisson channel in a controlled laboratory environment. Hashmi et al. [10] develop the Mars–Earth FSO channel under the Poisson model and analyze the link budget. Moreover, the FSO channel modeling needs take into account the solar scintillation effect [11], [12], which can lead to amplitude fluctuation of the received optical signal. Xu and Zeng [13] study the effect of amplitude fluctuation caused by coronal turbulence on the propagation of optical waves in superior solar conjunction. Hence, we need to establish the deep space FSO channel model that takes into account solar scintillation over a synodic period.

Moreover, design an effective coding scheme to relieve the solar scintillation for reliable transmission is also of paramount importance [6], [14]. Staircase codes are proposed by Smith et al. in [15] and are constructed using the Bose–Chaudhuri–Hocquenghem (BCH) code to form the ladder blocks, which are capable of parallel encoding and decoding. Component codes such as BCH codes [16], [17],

low density parity check (LDPC) codes, and other block codes [18] can be used in staircase codes. Staircase LDPC codes have shown excellent performance for high-speed optical transmission [19], which can provide a gain of 0.5–1 dB compared to staircase BCH codes [20]. Further, the staircase BCH code concatenated with low density generator matrix (LDGM) codes are proposed in [21] and [22], and with LDPC codes is proposed in [23], which can utilize the soft decoding for higher reliability.

In terms of decoding the staircase codes, the stall patterns are the main reason for the error floor [15]. Holzbaur et al. [24] locate the stall patterns by intersecting nonzero syndromes and solve it by a bit-flipping scheme, where each bit in the staircase structure is protected by two codewords. Moreover, hard-decision decoding algorithm is applied to the BCH component codes in the sliding window algorithm (SWD), which is not appreciable for LDPC component codes [25]. Wijekoon et al. [20] propose a belief propagation (BP) algorithm-based SWD with bit-flipping for staircase LDPC codes. However, the bit flipping scheme cannot decode the staircase code with the length of the reencoded bits is smaller than that of the staircase block. Zhang and Djordjevic [19] propose the rate-adaptive staircase LDPC codes with sequentially decoding to achieve more flexible code rate. Consider that the reencoded bits overlap in two adjacent staircase blocks, the reliability of the reencoded bits could be higher than the original reliability in the second block. However, there is still a lack of work to provide a specific decoding algorithm that utilizes the high reliability of reencoded bits.

The ordered statistics decoder (OSD) was proposed in 1995 [26], and it has been proven that for a linear block code with a minimum distance of D_{\min} , the OSD with order $M = \lceil D_{\min}/4 - 1 \rceil$ can approximate the maximum likelihood decoding performance. The skip and stop criteria are proposed in [27] and [28] to avoid those candidate codewords that are unlikely to be the correct output and reduce the complexity. Wang et al. [29] propose an adjustable OSD algorithm, which reduces decoding complexity by using reasonable thresholds based on the test error pattern (TEP) likelihood and weighted Hamming distance (WHD). Furthermore, Yue et al. [30] provide a comprehensive analysis of the OSD algorithm. Soft OSD (SOSD) [31] is a variant of OSD and modifies the output of OSD into soft information. Yue et al. [32] propose a low-complexity SOSD algorithm with a similar mutual information transform property to the original SOSD, and the decoding stop condition can effectively reduce complexity. Therefore, we can utilize the OSD to design corresponding decoder for the staircase LDPC codes over the synodic period FSO channel.

In this article, we propose an end-to-end FSO communication coding scheme for deep space exploration. Specifically, our contributions are as follows.

- 1) We analyze the solar scintillation effects on the FSO channel between the space station and planetary orbiter caused by the revolution of the Earth and Mars, and divide the FSO channel into three states

according to the scintillation index. 1) No scintillation state, where the Mars–Earth line-of-sight (LOS) link follows AWGN distribution. 2) Scintillation state, where the Mars–Earth LOS link is affected by the solar scintillation, and the FSO channel follows the Gamma-Gamma (GG) distribution, which is further divided into weak/moderate/strong scintillation. 3) Outage state, where the LOS link is blocked by the Sun due to the saturated scintillation. Then, we establish a synodic period channel model for the entire synodic period of Mars–Earth, and derive the upper bound of BER expressions for L -ary pulse position modulation (LPPM) under both AWGN and scintillation state fading channels.

- 2) We introduce the staircase LDPC codes to relieve the solar scintillation effects on the synodic period channel, and design two decoding algorithms for staircase LDPC codes with LPPM under both AWGN and scintillation state fading channels, named staircase code-OSD (SC-OSD) and SOSD-SWD algorithms. The SC-OSD algorithm modifies the input of conventional OSD according to the reencoded bits of staircase LDPC codes, which improves the reliability of the reencoded bits in OSD and can lower the output BER. Moreover, we derive the probability density function (PDF) and Gaussian approximation of the ordered statistics of the SC-OSD algorithm, which provide a guideline to derive a lower bound of block error rate (BLER) and reduce the decoding complexity of SC-OSD.
- 3) We introduce the SOSD as an inner iterative decoder for staircase LDPC codes under scintillation state fading channels, and propose the SOSD-SWD algorithm to address the error floor in conventional SWD decoder. Moreover, extensive simulations are conducted to show the BER performance under different parameters, including the window size and maximum numbers of outer iterations of the SWD decoder, and the order and maximum numbers of inner iterations of SOSD for staircase LDPC codes under different turbulence conditions. Simulation results demonstrate that compare to the conventional BP-SWD schemes, our SOSD-SWD can achieve a lower BER under different turbulence conditions.

The rest of this article is organized as follows. In Section II, we introduce the communication system model, including the synodic period channel model and the staircase LDPC encoding process, and derive the upper bound of BER for LPPM. Section III of this article describes the OSD algorithm, the proposed SC-OSD algorithm, and the proposed SOSD-SWD algorithm. Simulation results are presented in Section IV, which examines the performance of SC-OSD in no scintillation state, the performance of SOSD-SWD in scintillation state, and the investigation of the impact of different parameters on SOSD-SWD under different

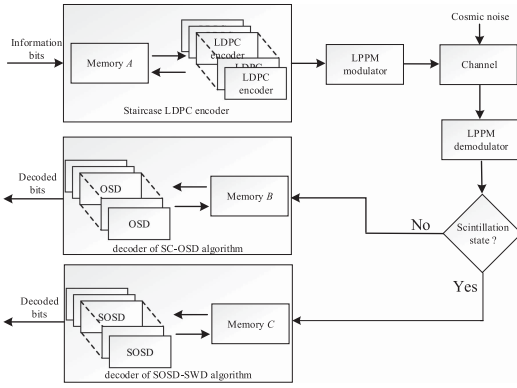


Fig. 1. End-to-end staircase LDPC encoder and the corresponding decoder for the deep space optical communications. At the encoder side, the memory A stores the reencoded bits of staircase LDPC codes, then the encoded bits update A for subsequent staircase block encoding, and sent to the LPPM modulator. At the decoder side, the proposed decoder of SC-OSD algorithm or proposed decoder of SOSD-SWD algorithm is selected based on the channel state. For decoder of SC-OSD algorithm, the memory B stores the modified reliabilities of the reencoded bits from the previous staircase block. For decoder of SOSD-SWD algorithm, the memory C stores the demodulated soft information values and a priori values of all staircase blocks within the current window.

turbulence conditions. Finally, Section V concludes this article.

II. SYSTEM MODEL

The block diagram of the end-to-end staircase LDPC encoder and the corresponding decoder for the deep space optical communications is shown in Fig. 1.

A. Synodic Period FSO Channel Modeling

The deep space optical communications are susceptible to interference from coronal turbulence due to the solar activity, which leads to significant degradation. The GG distribution is widely used to model the turbulence conditions from weak to strong on the FSO link, and its PDF is given by [33]

$$f_I(x) = \frac{2(\phi\varphi)^{\frac{(\phi+\varphi)}{2}}}{\Gamma(\phi)\Gamma(\varphi)} x^{\frac{(\phi+\varphi)}{2}-1} K_{\phi-\varphi}\left(2\sqrt{\phi\varphi}x\right), x > 0 \quad (1)$$

where K_x is the modified Bessel function of second kind with order x , Γ is the standard Gamma function, $\phi > 0$ and $\varphi > 0$ are the effective numbers of large- and small-scale scatterers, which can be expressed as functions of the variance of amplitude fluctuations χ^2 [34]

$$\phi = \left\{ \exp \left[\frac{0.49\chi^2}{(1 + 0.18d^2 + 0.56\chi^{12/5})^{7/6}} \right] - 1 \right\}^{-1} \quad (2)$$

and

$$\varphi = \left\{ \exp \left[\frac{0.51\chi^2 (1 + 0.69\chi^{12/5})^{-5/6}}{1 + 0.9d^2 + 0.62d^2\chi^{12/5}} \right] - 1 \right\}^{-1} \quad (3)$$

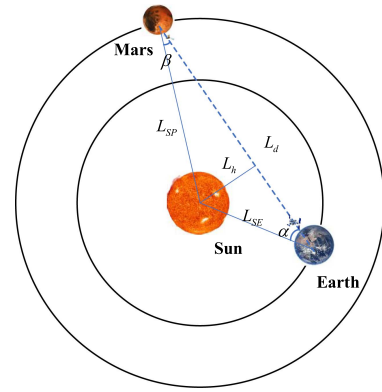


Fig. 2. System model of Earth to Mars communications around the Sun under coronal turbulence.

where $d = \sqrt{\frac{\pi D^2}{2\lambda L}}$, D represents the diameter of the receiver aperture, λ is the wavelength of FSO signal and we choose 1550 nm in this article [4].

The closed-form expression of χ^2 can be derived by utilizing the non-Kolmogorov turbulence model with the Rytov approximation method, and we have [35]

$$\chi^2 = \frac{2^{\frac{p-9}{2}} \pi^{\frac{p+1}{2}} r_e^2 p(p-3) \Gamma\left(\frac{p}{2}\right) \zeta^2 N_e^2(L_h) L_o^{3-p} L_d^{\frac{p+2}{2}} \lambda^{\frac{p+2}{2}}}{\Gamma\left(\frac{p-1}{2}\right) \Gamma\left(\frac{p+1}{2}\right)}, \quad (4)$$

where $3 < p < 4$ is the spectral index, r_e is the classical electron radius, L_d is the optical link distance, L_o is the outer scale of coronal turbulence, ζ is the relative solar wind density fluctuations coefficient, and N_e is the solar wind density. We adopt the widely used Smith and Ho model [36], $N_e(L_h) = 2.21 \times 10^{14} \left(\frac{R_{\text{sun}}}{L_h}\right)^6 + 1.55 \times 10^{12} \left(\frac{R_{\text{sun}}}{L_h}\right)^{2.3}$, where R_{sun} is the solar radius, and L_h is the shortest distance from the Sun to the FSO link.

Then, we take the Tianwen Mars orbiter to model the synodic period FSO channel as shown in Fig. 2, where both the orbiter and Earth are around the Sun, L_{SE} is the average distance from Earth to Sun, L_{SP} is the average distance from Mars to Sun, α is the SEP (Sun-Earth-Probe) angle, β is the SPE (Sun-Probe-Earth) angle. Obviously, we can directly calculate L_d by the geometric relationships of α and β as follows:

$$L_d = L_{SE} \cos \alpha + L_{SP} \cos \beta. \quad (5)$$

Moreover, the scintillation index σ_I^2 is defined to characterize the scintillation intensity of the Sun, which is the ratio of the root mean square value of the fluctuation of the signal intensity to the average value of the signal intensity I , and we have $\sigma_I^2 = \frac{\mathbb{E}[I^2]}{(\mathbb{E}[I])^2} - 1$ ($0 < \sigma_I^2 \leq 1$). For the GG distribution, σ_I^2 can be expressed as [8]

$$\sigma_I^2 = \frac{1}{\phi} + \frac{1}{\varphi} + \frac{1}{\phi\varphi}. \quad (6)$$

The influence of coronal turbulence on the FSO link varies due to α and β , and affects σ_I^2 as shown in (2)–(6) as shown in Fig. 3. Therefore, the FSO channel can be modeled

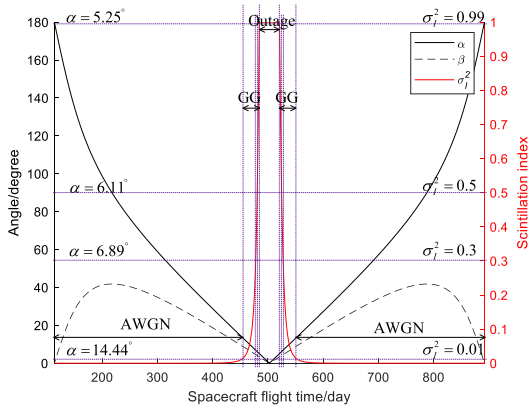


Fig. 3. Variation of α , β and corresponding σ_f^2 of the Mars-Earth synodic period.

TABLE I
Mars-Earth Synodic Period FSO Channel

Scintillation index	SEP	Channel model (state)	Duration
$\sigma_f^2 < 0.01$	$\alpha > 14.44^\circ$	AWGN	676 days
$0.01 < \sigma_f^2 < 0.3$	$6.89^\circ < \alpha < 14.44^\circ$	GG (weak scintillation)	54 days
$0.3 < \sigma_f^2 < 0.5$	$6.11^\circ < \alpha < 6.89^\circ$	GG (moderate scintillation)	6 days
$0.5 < \sigma_f^2 < 0.99$	$5.25^\circ < \alpha < 6.11^\circ$	GG (strong scintillation)	6 days
$\sigma_f^2 > 0.99$	$\alpha < 5.25^\circ$	outage	38 days

according to the value variations of σ_f^2 in a synodic period. Specifically, when the Earth and Mars are on opposite sides of Sun, we have $\sigma_f^2 > 0.99$ and the FSO link loses the LOS, and can be considered as outage. Moreover, when $\sigma_f^2 < 0.01$, the optical signal is minimally affected by solar activity, and the channel can be approximated as an AWGN channel. Finally, when $0.01 \leq \sigma_f^2 \leq 0.99$, the optical signal is affected by coronal turbulence, and we further divide the scintillation state of the FSO channel model into three states according to the value of σ_f^2 : 1) weak scintillation for $0.01 < \sigma_f^2 < 0.3$; 2) moderate scintillation for $0.3 < \sigma_f^2 < 0.5$; 3) strong scintillation for $0.5 < \sigma_f^2 < 0.99$. The corresponding SEP and durations for different channel states in a synodic period is summarized in Table I.

B. BER Derivation of Uncoded Synodic Period FSO Channel

In this subsection, we derive the BER of uncoded binary pulse position modulation (BPPM) and the upper bound BER of uncoded LPPM over the synodic period FSO channel, respectively.

At the transmitter, the uncoded binary bit b is modulated using LPPM. Moreover, every $\lceil \log_2 L \rceil$ binary bits grouped together are modulated into a LPPM symbol $\mathbf{x} = [x_1, x_2, \dots, x_L]$ composed of L slots, in which one of the slots equals 1 and the other slots equal 0 (i.e., 1 pulse slot and $(L - 1)$ noise slots). Specifically, BPPM is the case $L = 2$ of LPPM. Then, the channel output $\mathbf{r} = [r_1, r_2, \dots, r_L]$ can be expressed as

$$\mathbf{r} = \mathbf{h}\mathbf{x} + \mathbf{n} \quad (7)$$

where $\mathbf{h} = [h_1, h_2, \dots, h_L]$ is the channel coefficient vector, and $\mathbf{n} = [n_1, n_2, \dots, n_L]$ is the independent AWGN vector, where $n_i \sim \mathcal{N}(0, \sigma_n^2)$. Without loss of generality,

we consider the transmitter to send an all-zero signal, specifically

$$r_i = \begin{cases} h + n_i, & i = 1, \\ n_i, & i = 2, 3, \dots, L. \end{cases} \quad (8)$$

Furthermore, the received symbol is demodulated by comparing the amplitude of all slots in each symbol, and determining the slot with the largest amplitude as a pulse slot [37], [38].

Then, we derive the BER of uncoded BPPM $P_{e,B}$ and the upper bound BER of uncoded LPPM $P_{e,L}$ over the synodic period FSO channel in the following. With the help of the Meijer G-function to express $K_v(\sqrt{z})$ in (1) as $K_v(\sqrt{z}) = \frac{1}{2}G_{0,2}^{2,0}(\frac{z}{4}|_{v/2, -v/2})$ [39, eq. (03.04.26.0009.01)], we can rewrite (1) as

$$f_I(h) = \frac{(\phi\varphi)^{\frac{(\phi+\varphi)}{2}}}{\Gamma(\phi)\Gamma(\varphi)} h^{\frac{(\phi+\varphi)}{2}-1} G_{0,2}^{2,0}\left(\phi\varphi h \middle|_{\frac{\phi-\varphi}{2}, \frac{\varphi-\phi}{2}}\right), h > 0. \quad (9)$$

Then, the conditional BER of BPPM is represented as

$$P_e(h) = Q\left(\frac{h}{\sqrt{2\sigma_n^2}}\right). \quad (10)$$

Moreover, note that $Q(\sqrt{z}) = \frac{1}{2}\text{erfc}(\frac{\sqrt{z}}{2})$ and by utilizing $\text{erfc}(\sqrt{z}) = \frac{1}{\sqrt{\pi}}G_{2,0}^{1,2}(z|_{0, \frac{1}{2}})$ [39, eq. (06.27.26.0006.01)], (10) can be expressed as

$$P_e(h) = \frac{1}{\sqrt{2\pi}}G_{2,0}^{1,2}\left(\frac{h^2}{4\sigma_n^2} \middle|_{0, \frac{1}{2}}\right). \quad (11)$$

Thus, when $5.25^\circ < \alpha < 14.44^\circ$, the average BER in the synodic period channel under BPPM can be calculated as

$$P_{e,B} = \int_0^\infty P_e(h)f_I(h)dh. \quad (12)$$

Then, we can derive the closed-form of the above integral (12) according to [39, eq. (07.34.21.0012.01)],

$$P_{e,B} = \frac{1}{2\sqrt{\pi}\Gamma(\phi)\Gamma(\varphi)} H_{3,2}^{2,2}\left(\left(\frac{1}{2\sigma_n\phi\varphi}\right)^2 \middle|_{(0,1), (\frac{1}{2}, 1)}^{(1-\phi, 2), (1-\varphi, 2), (1, 1)}\right) \quad (13)$$

where H represent the Fox H function.

Note that $\alpha > 14.44^\circ$ in the most time of the synodic period as shown in Table I, and (12) can be simplified as

$$P_{e,B} = Q\left(\frac{1}{\sqrt{2\sigma_n^2}}\right). \quad (14)$$

Further, the upper bound BER of uncoded LPPM $P_{e,L}$ over FSO channel can be expressed as [37]

$$P_{e,L} = \frac{L}{2(L-1)} \left(1 - (1 - P_{e,B})^{L-1}\right) \quad (15)$$

and by substituting (13) into (15), the upper bound to the average BER of LPPM can be calculated as (16) shown at

TABLE II
Simulation Parameters Under Different Turbulent Conditions

Turbulent conditions	σ_7^2	α	ϕ	φ
Weak scintillation	0.2	7.56°	10.77	10.21
Moderate scintillation	0.4	6.47°	5.67	5.26
Strong scintillation	0.8	5.43°	3.13	2.75

the bottom of the next page when $5.25^\circ < \alpha < 14.44^\circ$, and for $\alpha > 14.44^\circ$, we have

$$P_{e,L} = \frac{L}{2(L-1)} \left(1 - \left(1 - Q \left(\frac{1}{\sqrt{2\sigma_n^2}} \right) \right)^{L-1} \right). \quad (17)$$

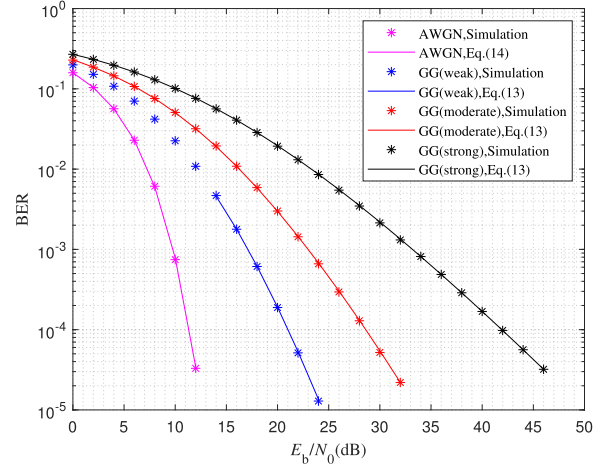
We compare the Monte Carlo simulation results of BER over the FSO channel with turbulent conditions from Table II to our derived expressions as shown in Fig. 4. In Fig. 4(a), the curves from the closed-form expressions of BER under BPPM agree well with the simulation results. Moreover, the upper bound BER under 4PPM are approaching the simulation results in the weak and moderate scintillations as shown in Fig. 4(b), which also validate the accuracy of our derivations. Further, we can observe that the GG channel under weak scintillation requires about 10 dB higher SNR than that of AWGN channel to achieve $\text{BER} \leq 10^{-4}$, while requiring 30 dB higher SNR under strong scintillation. Therefore, we should design an effective coding scheme to resolve performance loss caused by the solar scintillation and reduce the requirement for transmission power.

C. Staircase LDPC Encoding

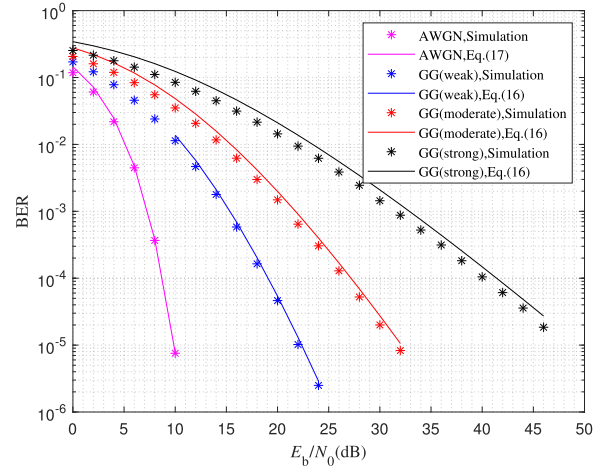
In this article, the systematic LDPC code $\mathcal{C}(N, K)$ with the codeword length of N , the message bits length of K and generator matrix \mathbf{G} is selected as the component code of the staircase codes, and the encoding process of the staircase LDPC codes is shown in Fig. 5(a), where m is the length of reencoded bits, T represents the matrix transpose, and \mathbf{B}_i represents the i th block of the staircase code.

The encoding process of staircase LDPC codes starts from \mathbf{B}_1 and proceeds sequentially in a forward order. The $m \times (N - m)$ matrix \mathbf{B}_0 is initialized to an all-zero matrix, which is known to the receiver and does not send over the channel. $\mathbf{B}_1, \mathbf{B}_2, \mathbf{B}_3 \dots$ all are matrices of size $(N - m) \times (N - m)$.

For example, taking the encoding process of the V th block $\mathbf{B}_V = [\mathbf{B}_{V, \text{message}}, \mathbf{B}_{V, \text{parity}}]$ as shown in Fig. 5(b), where $\mathbf{B}_{V, \text{message}}$ is the information bit submatrix of size $(N - m) \times (K - m)$, and $\mathbf{B}_{V, \text{parity}}$ is the parity check bit submatrix of size $(N - m) \times (N - K)$. Note that the submatrix $\mathbf{B}_{V-1, \text{re}}$ of size $(N - m) \times m$ is the rightmost m -column of \mathbf{B}_{V-1}^T , which is the reencoded bit submatrix for \mathbf{B}_V .



(a)



(b)

Fig. 4. Uncoded BER under synodic period channel. (a) Uncoded theoretical average BER and simulation BER under BPPM. (b) Upper bound of uncoded theoretical average BER and simulation BER under 4PPM.

Specifically, a staircase LDPC encoder requires $(N - m)$ LDPC encoders operating in a parallel manner, and a memory cell can store the reencoded submatrix of the previous block. The first step is to generate $\mathbf{B}_{V, \text{message}} = [\mathbf{u}_1^V, \mathbf{u}_2^V, \dots, \mathbf{u}_{N-m}^V]^T$, where $\mathbf{u}_i^V = [b_{i,1}^V, b_{i,2}^V, \dots, b_{i,K-m}^V]$, and $b_{i,j}^V \in \{0, 1\}$ represents the bit of the i th row and the j th column of the V th block. Next, the encoder reads $\mathbf{B}_{V-1, \text{re}} = [\mathbf{u}_1'^{V-1}, \mathbf{u}_2'^{V-1}, \dots, \mathbf{u}_{N-m}'^{V-1}]^T$ from the memory cell, where $\mathbf{u}_i'^{V-1} = [b_{N-2m+1,i}^{V-1}, b_{N-2m+2,i}^{V-1}, \dots, b_{N-m,i}^{V-1}]$. At this point, the input $\tilde{\mathbf{u}}_i^V = [\mathbf{u}_i'^{V-1}, \mathbf{u}_i^V]$ of the LDPC encoder is obtained. Finally, we obtain $\mathbf{B}_{V, \text{parity}}$ by the parallel encoding $\mathbf{c}_i^V = \tilde{\mathbf{u}}_i^V \cdot \mathbf{G}$, where $1 \leq i \leq N - m$.

$$P_{e,L} = \frac{L}{2(L-1)} \left(1 - \left(1 - \frac{1}{2\sqrt{\pi}\Gamma(\phi)\Gamma(\varphi)} H_{3,2}^{2,2} \left(\left(\frac{1}{2\sigma_n\phi\varphi} \right)^2 \left|_{(0,1), (\frac{1}{2}, 1)}^{(1-\phi, 2), (1-\varphi, 2), (1, 1)} \right. \right) \right)^{L-1} \right) \quad (16)$$

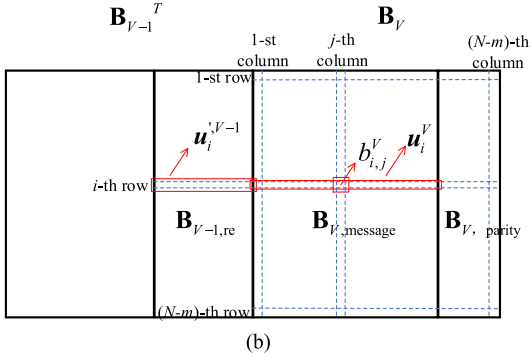
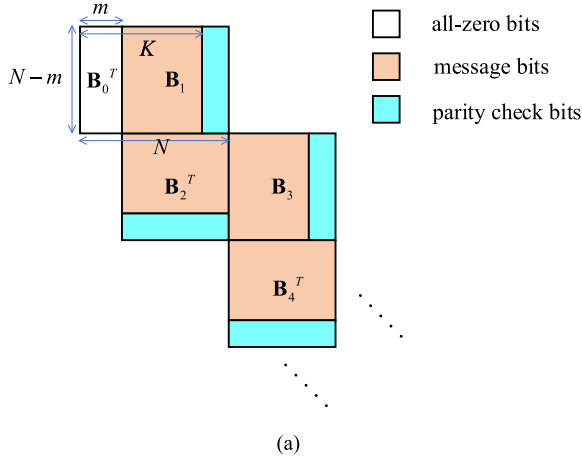


Fig. 5. Encoding structure of the staircase LDPC codes. (a) Nonterminating encoding process of the staircase code. (b) Encoding process of the V th block \mathbf{B}_V .

III. DECODING ALGORITHM

In this section, we propose two decoding algorithms for staircase LDPC codes: 1) low-complexity SC-OSD algorithm for AWGN channels, and 2) the high-reliability SOSD-SWD algorithm for GG fading channels.

A. OSD

To simplify the analysis, we neglect the distinction between different staircase blocks and different codewords in different rows, and omit the superscript V and subscript i . Let $\mathbf{c} = [c_1, c_2, \dots, c_N]$ denote the encoding codeword sequence, and note that $\mathbf{c}_{1:m} = [c_1, c_2, \dots, c_m]$ and $\mathbf{c}_{m+1:N} = [c_{m+1}, c_{m+2}, \dots, c_N]$ are modulated and transmitted separately for different staircase blocks.

The staircase blocks are modulated through BPPM, where 0 is modulated to $[1, 0]$ and 1 is modulated to $[0, 1]$. We define $\mathbf{r}_i = [r_{i,1}, r_{i,2}]$ as the i th received symbol, where $1 \leq i \leq N$. The received signal over the AWGN channel is

$$r_{i,j} = \begin{cases} 1 + n_{i,1}, & j = 1 \\ n_{i,2}, & j = 2 \end{cases} \quad (18)$$

where $n_{i,1}$ and $n_{i,2}$ are independent and identically distributed AWGN noises with $\mathcal{N}(0, \sigma_n^2)$. After demodulating,

we have $\mathbf{y} = [y_1, y_2, \dots, y_N]$, where

$$y_i = \begin{cases} 0, & r_{i,1} > r_{i,2} \\ 1, & r_{i,1} < r_{i,2}. \end{cases} \quad (19)$$

The log likelihood ratio (LLR) can be calculated as $\delta_i = \frac{(r_{i,1} - r_{i,2})}{\sigma_n^2}$. Then, the reliability sequence is defined as $\mathbf{o} = [o_1, o_2, \dots, o_N]$, where $o_i = |r_{i,1} - r_{i,2}|$.

The main steps of the OSD algorithm are as follows. Initially, the reliability sequence \mathbf{o} is arranged in descending order to obtain the first column permutation Π_1 , $\bar{\mathbf{o}} = [\bar{o}_1, \bar{o}_2, \dots, \bar{o}_N]$, and $\bar{o}_1 > \bar{o}_2 > \dots > \bar{o}_N$ can be obtained. Thus, $\bar{\mathbf{y}} = \Pi_1(\mathbf{y})$ and $\bar{\mathbf{G}} = \Pi_1(\mathbf{G})$.

Next, the Gaussian elimination is performed on $\bar{\mathbf{G}}$ to obtain the systematic generator matrix $\tilde{\mathbf{G}}$, which corresponds to the second permutation Π_2 for ensuring linear independence of the first K columns in $\tilde{\mathbf{G}}$. Thus, $\tilde{\mathbf{y}} = \Pi_2(\bar{\mathbf{y}})$ and $\tilde{\mathbf{o}} = \Pi_2(\bar{\mathbf{o}})$. The OSD takes the first K bits of $\tilde{\mathbf{y}}$ and denoted as $\tilde{\mathbf{y}}_B$, which is the most reliable basis (MRB). The remaining $(N - K)$ bits is the least reliable basis (LRB).

Finally, the reencoding operation is performed on $\tilde{\mathbf{y}}_B$ through TEP \mathbf{e} to obtain the candidate codeword $\tilde{\mathbf{c}}_e = (\tilde{\mathbf{y}}_B \oplus \mathbf{e})\tilde{\mathbf{G}}$. For the OSD with order M , in the stage-0 reprocessing, there is no error in $\tilde{\mathbf{y}}_B$, i.e., $\tilde{\mathbf{c}}_e = \tilde{\mathbf{y}}_B\tilde{\mathbf{G}}$. In the stage- i ($1 \leq i \leq M$), the TEPs with Hamming weight of i are checked in dictionary order. The TEP likelihood for \mathbf{e} is defined as [27]

$$\mathcal{L}_e \triangleq \sum_{1 \leq i \leq K, e_i=1} \tilde{o}_i. \quad (20)$$

Further, let $\Lambda = \sum_{i=0}^M \binom{K}{i}$ denote the number of TEPs need to be checked, and the codeword with the minimum WHD D_e is selected from all Λ candidate codewords, which is denoted as the optimal estimated codeword $\hat{\mathbf{c}}$, and

$$D_e = \sum_{\substack{1 \leq i \leq N \\ \tilde{\mathbf{c}}_{e,i} \neq \tilde{y}_i}} \tilde{o}_i. \quad (21)$$

Therefore, the output result of OSD is $\Pi_2^{-1}(\Pi_1^{-1}(\hat{\mathbf{c}}))$.

B. SC-OSD

In this subsection, we first modify the OSD based on the structure of staircase LDPC codes and propose the SC-OSD algorithm. Next, we derive the expressions for ordered statistics in SC-OSD and obtain the lower bound of BLER. Finally, we prove the Gaussian approximation of ordered statistics and reduce the complexity of SC-OSD by the TEP skip criterion.

When the receiver decodes \mathbf{B}_V , the input to the decoder is $[\mathbf{B}_{V-1, re}, \mathbf{B}_V]$, where $\mathbf{B}_{V-1, re}$ has already obtained its estimation during the decoding of the previous staircase block \mathbf{B}_{V-1} . Evidently, the reliability of the decoded bits is expected to be higher than that of the undecoded bits, so a reliability factor $\mu > 1$ is introduced. We define the reliability sequence of SC-OSD as $\mathbf{o}' = [o'_1, o'_2, \dots, o'_N]$,

where

$$o'_i = \begin{cases} \mu o_i, & 1 \leq i \leq m \\ o_i, & m+1 \leq i \leq N. \end{cases} \quad (22)$$

The last $(N - m)$ bits of the SC-OSD decision sequence $\mathbf{y}' = [y'_1, y'_2, \dots, y'_N]$ are determined by the demodulator, while the first m bits are determined by the previous estimation result, thus

$$y'_i = \begin{cases} \hat{y}_i, & 1 \leq i \leq m \\ y_i, & m+1 \leq i \leq N \end{cases} \quad (23)$$

where \hat{y}_i denotes the optimal estimation of the i th bit during the decoding of the previous blocks.

For $m+1 \leq i \leq N$, the PDF of o'_i is

$$f_o(x) = \begin{cases} 0, & \text{if } x < 0 \\ \frac{e^{-\frac{(x+1)^2}{4\sigma_n^2}}}{\sqrt{4\pi\sigma_n^2}} + \frac{e^{-\frac{(x-1)^2}{4\sigma_n^2}}}{\sqrt{4\pi\sigma_n^2}}, & \text{if } x \geq 0 \end{cases} \quad (24)$$

and the cumulative distribution function (CDF) is

$$F_o(x) = \begin{cases} 0, & \text{if } x < 0 \\ 1 - Q\left(\frac{x+1}{\sqrt{2\sigma_n^2}}\right) - Q\left(\frac{x-1}{\sqrt{2\sigma_n^2}}\right), & \text{if } x \geq 0. \end{cases} \quad (25)$$

Similarly, for $1 \leq i \leq m+1$, the PDF of o'_i is

$$f_{o'}(x) = \begin{cases} 0, & \text{if } x < 0 \\ \frac{e^{-\frac{(x+\mu)^2}{4\mu^2\sigma_n^2}}}{\sqrt{4\pi\mu^2\sigma_n^2}} + \frac{e^{-\frac{(x-\mu)^2}{4\mu^2\sigma_n^2}}}{\sqrt{4\pi\mu^2\sigma_n^2}}, & \text{if } x \geq 0 \end{cases} \quad (26)$$

and the CDF is

$$F_{o'}(x) = \begin{cases} 0, & \text{if } x < 0 \\ 1 - Q\left(\frac{x+\mu}{\sqrt{2\mu^2\sigma_n^2}}\right) - Q\left(\frac{x-\mu}{\sqrt{2\mu^2\sigma_n^2}}\right), & \text{if } x \geq 0. \end{cases} \quad (27)$$

By sorting \mathbf{o}' in descending order, we obtain the ordered statistic $\tilde{\sigma}' = [\tilde{\sigma}'_1, \tilde{\sigma}'_2, \dots, \tilde{\sigma}'_N]$, $\tilde{\sigma}'_1 > \tilde{\sigma}'_2 > \dots > \tilde{\sigma}'_N$, whose PDF on the u th position is given by

$$f_{\tilde{\sigma}'_u}(x) = f_{\tilde{\sigma}'_{u,1}}(x) + f_{\tilde{\sigma}'_{u,2}}(x) \quad (28)$$

where $f_{\tilde{\sigma}'_{u,1}}(x)$ and $f_{\tilde{\sigma}'_{u,2}}(x)$ are given by (29) and (30) shown at the bottom of this page, respectively.

To simplify the analysis, we assume that errors in the first m bits of \mathbf{y}' for SC-OSD have already been corrected. In other words, $\hat{y}_i = 0$ if the all-zero signal is transmitted. Therefore, conditioning on $\tilde{\sigma}'_{K+1} = x$, the probability of j errors in the MRB \mathbf{y}'_B is given by

$$p_E(j | x) = \sum_{i=0}^m \binom{K-i}{j} \binom{m}{i} (1-p(x))^{K-m-j} \cdot p(x)^j (1-F_{o'}(x))^i (F_{o'}(x))^{m-i} \quad (31)$$

where $p(x) = \frac{Q(\frac{x+1}{\sqrt{2\sigma_n^2}})}{1+Q(\frac{x+1}{\sqrt{2\sigma_n^2}}) - Q(\frac{-x+1}{\sqrt{2\sigma_n^2}})}$. Finally, the probability of j errors in the MRB can be expressed as [30]

$$p_E(j) = \int_0^\infty p_E(j | x) f_{\tilde{\sigma}'_{K+1}}(x) dx. \quad (32)$$

Under the condition that $\hat{y}_i = 0$, Fig. 6 verifies the probability mass function of $p_E(j)$ for staircase LDPC codes at different SNRs. However, the fact is that errors may still exist in the first m bits of \mathbf{y}' . Therefore, the lower bound of the BLER for SC-OSD with order M can be expressed as follows:

$$P_{\text{lower}} = 1 - \sum_{j=0}^M p_E(j). \quad (33)$$

We compare the theoretical lower bound and the simulation results of the staircase LDPC codes for different M in Fig. 7. It can be observed that at low SNR, there is a significant difference between the theoretical performance and the simulation results, which is attributed to the assumption of $\hat{y}_i = 0$. Therefore, μ may lead to an increase in the reliability of error bits and degrade the decoding performance, especially at low SNR. Thus, we simulate the BLER performance under different SNR versus μ as shown in Fig. 8, and we can observe that the optimal value of μ increases with the SNR.

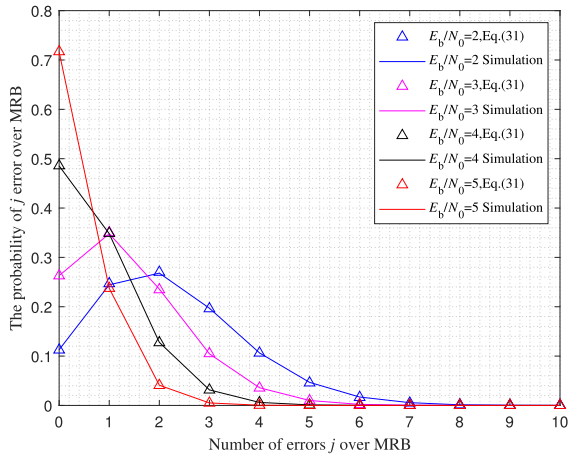
Similar to the traditional OSD algorithm [30], we can also use the central limit theorem to approximate the ordered reliability $\tilde{\sigma}'_u$ in the SC-OSD algorithm. The PDF of $\tilde{\sigma}'_u$ follows the normal distribution $\mathcal{N}(\mathbb{E}[\tilde{\sigma}'_u], \sigma_{\tilde{\sigma}'_u}^2)$, which is

$$f_{\tilde{\sigma}'_{u,1}}(x) = \sum_{i=\max(0, u-m-1)}^{u-1} p_i (1-F_o(x))^i (F_o(x))^{N-m-i-1} (1-F_{o'}(x))^{u-i-1} (F_{o'}(x))^{m+i-u+1} f_o(x) \quad (29)$$

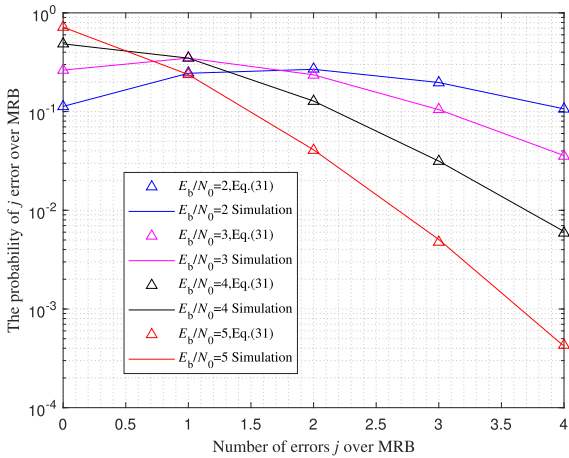
where $p_i = \binom{N-m}{i} \binom{m}{u-i-1} (N-m-i)$.

$$f_{\tilde{\sigma}'_{u,2}}(x) = \sum_{i=0}^{\min(m-1, u-1)} q_i (1-F_o(x))^{u-i-1} (F_o(x))^{N-m-u+i+1} (1-F_{o'}(x))^i (F_{o'}(x))^{m-i-1} f_o(x) \quad (30)$$

where $q_i = \binom{m}{i} \binom{N-m}{u-i-1} (m-i)$.



(a)



(b)

Fig. 6. Probability of j errors occurring over MRB in decoding the staircase LDPC codes at different SNRs with $N = 128$, $K = 64$, $m = 32$, $\mu = 2$. (a) Linear scale. (b) Logarithmic scale.

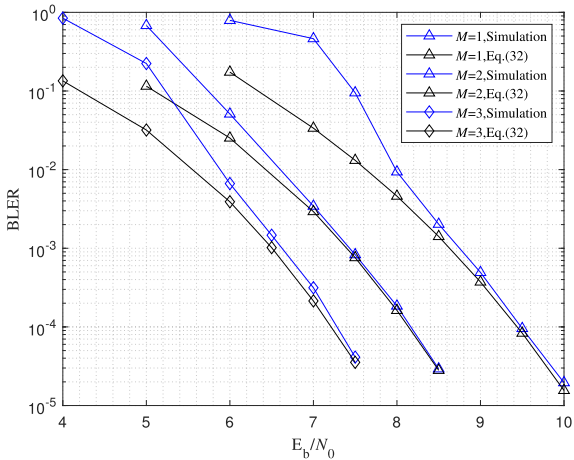


Fig. 7. BLER of SC-OSD for staircase LDPC codes with $N = 128$, $K = 64$, $m = 32$, $\mu = 2$.

given by

$$f_{\tilde{\sigma}_u}(x) \approx \frac{1}{\sqrt{2\pi\sigma_{\tilde{\sigma}_u}^2}} \exp\left(-\frac{(x - \mathbb{E}[\tilde{\sigma}_u])^2}{2\sigma_{\tilde{\sigma}_u}^2}\right) \quad (34)$$

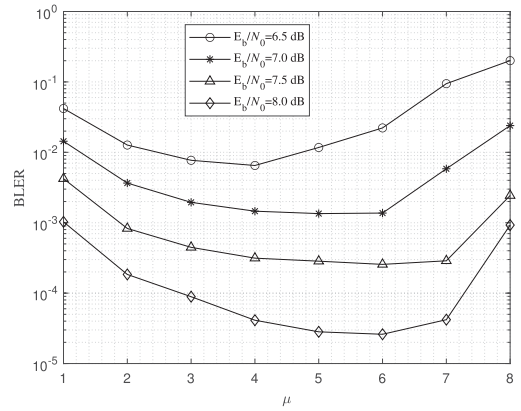


Fig. 8. BLER of SC-OSD for different μ values with $N = 128$, $K = 64$, $m = 32$.

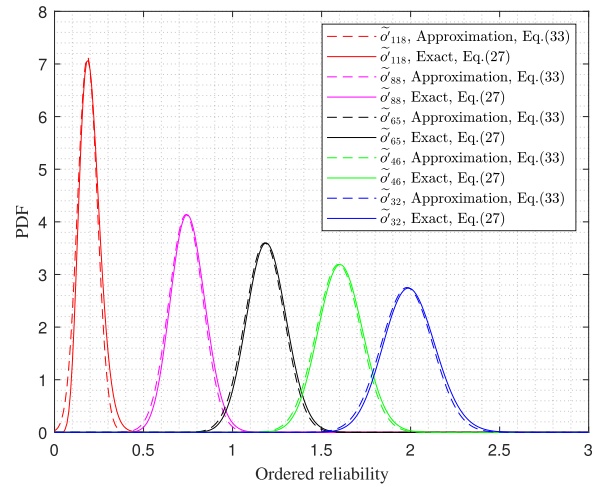


Fig. 9. Approximation of the distribution of ordered reliability with $N = 128$, $K = 64$, $m = 32$, $\mu = 2$, $E_b/N_0 = 5$ dB.

where the value of $\mathbb{E}[\tilde{\sigma}_u]$ satisfies the following equation uniquely:

$$\left(\frac{N-m}{N-u}\right) F_o(\mathbb{E}[\tilde{\sigma}_u]) + \left(\frac{m}{N-u}\right) F_{o'}(\mathbb{E}[\tilde{\sigma}_u]) = 1 \quad (35)$$

and

$$\sigma_{\tilde{\sigma}_u}^2 = \frac{N-u - (N-m)F_o(\mathbb{E}[\tilde{\sigma}_u])^2 - mF_{o'}(\mathbb{E}[\tilde{\sigma}_u])^2}{((N-m)f_o(\mathbb{E}[\tilde{\sigma}_u]) + mf_{o'}(\mathbb{E}[\tilde{\sigma}_u]))^2} \quad (36)$$

We show the exact distributions and approximation of the ordered statistics of SC-OSD in Fig. 9, and the specific derivation of $\mathbb{E}[\tilde{\sigma}_u]$ and $\sigma_{\tilde{\sigma}_u}^2$ can be found in Appendix A.

Then, we derive the distribution of likelihood for the correct TEP, and the distribution of likelihood for all TEPs to determine the threshold \mathcal{L}_{thr} for the skip criterion in the SC-OSD algorithm.

When the true error pattern TEP can be identified in the decoding process of the SC-OSD algorithm, the SC-OSD can eliminate errors in the MRB. The PDF of the correct

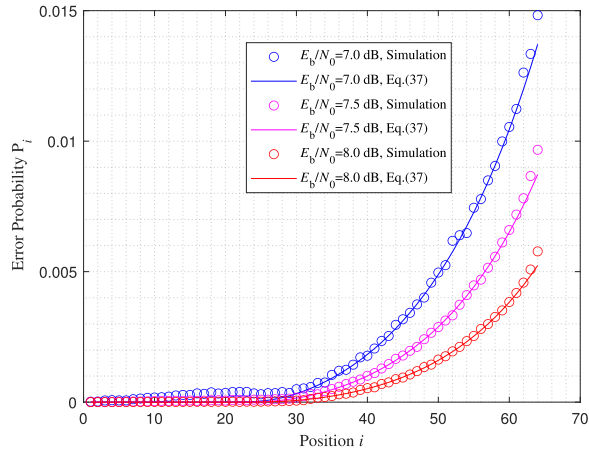


Fig. 10. Probability of error per bit in the MRB, $N = 128, K = 64, m = 32, \mu = 6$.

TEP likelihood for correct TEP e_B is as follows [29]:

$$f_{\mathcal{L}_{e_B}}(x) = \begin{cases} \frac{p_E(j=0)}{\sum_{j=0}^M p_E(j)}, & x = 0 \\ \sum_{j=0}^M \frac{p_{E_1^k}(j)}{p_{E_1^k}(0 \leq j \leq M)} \sum_{q=1}^{(q_{\max})} f_{\mathcal{G}_q}(x) \prod_{i \in \Psi_q^j} P_i, & x \neq 0 \end{cases} \quad (37)$$

where $\mathcal{G}_q \sim \mathcal{N}(E_q, \sigma_q^2)$, $f_{\mathcal{G}_q}(x)$ is the PDF of the variable \mathcal{G}_q , Ψ_q^j is the q th position index combination conditioning on number of errors j over MRB, $q_{\max} = \binom{K}{j}$ are the total sum of these possible combinations, P_i is the error probability of the i th position. Similarly, assume that $\hat{y}_i = 0$, and P_i can be expressed as

$$P_i = \int_0^\infty \frac{e^{-\frac{(x+1)^2}{4\sigma_i^2}}}{e^{-\frac{(x-1)^2}{4\sigma_i^2}} + e^{-\frac{(x+1)^2}{4\sigma_i^2}}} f_{\tilde{\sigma}_{i,1}}(x) dx. \quad (38)$$

Fig. 10 shows the theoretical and simulation results of P_i under different SNR, and we can observe that at high SNR, the theoretical and simulated results exhibit minimal differences due to the assumption conditions.

The PDF of likelihood of all TEPs is [29]

$$f_{\mathcal{L}_e}(x) = \frac{1}{\Lambda} \sum_{j=0}^M \sum_{q=1}^{q_{\max}} G_{E_q, \sigma_q^2}(x). \quad (39)$$

Fig. 11 compares the simulation and theoretical analysis about the PDF of likelihood for the correct TEP and all TEPs.

We set the parameters θ_{TEP} as follows:

$$\theta_{\text{TEP}} = \frac{1}{1 - f_{\mathcal{L}_{e_B}}(0)} \int_{0^+}^{\mathcal{L}_{\text{thr}}} f_{\mathcal{L}_{e_B}}(x) dx. \quad (40)$$

Therefore, we can find the corresponding \mathcal{L}_{thr} by the value of θ_{TEP} .

Finally, we summarize the binary operations (BOPs) as the computational complexity of our SC-OSD algorithm, which is mainly determined as follows.

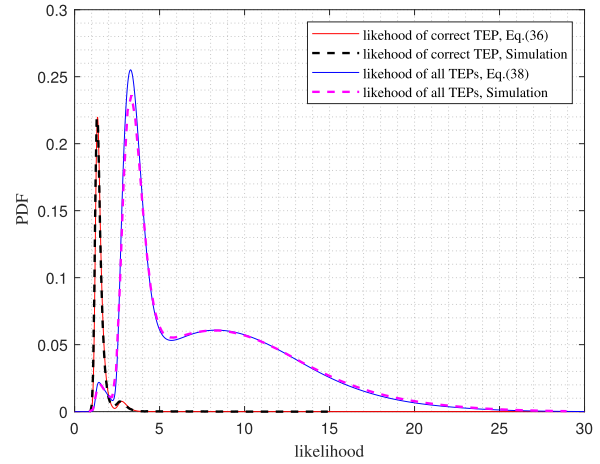


Fig. 11. Simulation and theoretical analysis about the PDF of likelihood for the correct TEP and all TEPs, $N = 128, K = 64, m = 32, \mu = 6, E_b/N_0 = 7.5$ dB.

1) The average complexity of obtaining Π_1 is $\mathcal{O}(N \log N)$ [40], [41].

2) The complexity of obtaining Π_2 by using smart Gaussian Elimination is $\mathcal{O}(N(N-K)^2)$ [42], [43].

3) The number of reencoding operations $R_n^{\text{SC-OSD}}$, which is determined by the TEP skip criterion [29], and the complexity of each reencoding is $\mathcal{O}(K + K(N-K))$ BOPs. Note that it is difficult to give the precise expression of $R_n^{\text{SC-OSD}}$, and we count it via Monte Carlo simulations in Section V. The total complexity of our SC-OSD algorithm is

$$T_{\text{SC-OSD}} \approx N \log N + N(N-K)^2 + R_n^{\text{SC-OSD}}(K + K(N-K)). \quad (41)$$

Define ψ_V^c as the LLR after demodulation of \mathbf{B}_V , and $\psi_{V,\text{re}}^c$ corresponds to the LLR of $\mathbf{B}_{V,\text{re}}$. Let $\mathbf{L}_V^c = [\psi_{V-1,\text{re}}^c, \psi_V^c] = [l_{V,1}^c, l_{V,2}^c, \dots, l_{V,N-m}^c]^T$, where $l_{V,i}^c$ is the i th row of matrix \mathbf{L}_V^c . The SC-OSD algorithm is summarized in Algorithm 1 in detail.

C. SOSD-SWD

In this subsection, we propose the SOSD-SWD algorithm for staircase LDPC codes to mitigate the impact of coronal turbulence on optical signals as $5.25^\circ < \alpha < 14.44^\circ$. Specifically, the main idea of the SOSD-SWD algorithm utilizes SOSD as the component code decoder in the SWD algorithm.

The SOSD is a soft output variant of OSD. Given the input LLR, $\mathbf{l}^{\text{in}} = [l^{\text{in}}(1), l^{\text{in}}(2), \dots, l^{\text{in}}(N)]$, the output LLR of SOSD $\mathbf{l}^{\text{out}} = [l^{\text{out}}(1), l^{\text{out}}(2), \dots, l^{\text{out}}(N)]$ can be calculated [44]

$$l^{\text{out}}(i) = \sum_{j=1}^N l^{\text{in}}(j) (\hat{c}_{i=0}(j) - \hat{c}_{i=1}(j)) \quad (42)$$

where $\hat{c}_{i=0} = [\hat{c}_{i=0}(1), \hat{c}_{i=0}(2), \dots, \hat{c}_{i=0}(N)]$ and $\hat{c}_{i=1} = [\hat{c}_{i=1}(1), \hat{c}_{i=1}(2), \dots, \hat{c}_{i=1}(N)]$ are the codeword estimations with the minimum WHD, whose i th bit is between 0

Algorithm 1: SC-OSD Algorithm.

Input: $\psi_1^c, \psi_2^c, \dots, \mathbf{G}, M, \mu$, the SNR γ , θ_{TEP}

Output: Optimal estimation $\tilde{\mathbf{B}}_1, \tilde{\mathbf{B}}_2, \dots$

- 1: Initialize $\tilde{\mathbf{B}}_0$ as all zeros
 - 2: Calculate \mathcal{L}_{thr} based on (40)
 - 3: **for** $V = 1, 2, \dots$ **do**
 - 4: $\psi_{V-1, re}^c = \mu \cdot |\psi_{V-1, re}^c| \cdot (-1)^{\tilde{\mathbf{B}}_{V-1, re}^c}$
 - 5: Obtain $\mathbf{L}_V^c = [\psi_{V-1, re}^c, \psi_V^c]$
 - 6: **for** $i = 1, 2, \dots, N - m$ **do**
 - 7: Obtain corresponding \mathbf{y}' and \mathbf{o}' by $\mathbf{L}_{V,i}^c$
 - 8: Perform the first permutation Π_1 :
 $\tilde{\mathbf{o}}' = \Pi_1(\mathbf{o}')$, $\tilde{\mathbf{y}}' = \Pi_1(\mathbf{y}')$, $\tilde{\mathbf{G}} = \Pi_1(\mathbf{G})$
 - 9: Perform the second permutation Π_2 :
 $\tilde{\tilde{\mathbf{G}}} = \Pi_2(\tilde{\mathbf{G}})$, $\tilde{\tilde{\mathbf{y}}}' = \Pi_2(\tilde{\mathbf{y}}')$, $\tilde{\tilde{\mathbf{o}}}' = \Pi_2(\tilde{\mathbf{o}}')$
 - 10: Perform the reencoding $\tilde{\tilde{\mathbf{c}}}_0 = \tilde{\tilde{\mathbf{y}}}' \cdot \tilde{\tilde{\mathbf{G}}}$
 - 11: Calculate WHD $D_{opt} = \sum_{\tilde{\tilde{\mathbf{c}}}_0, i \neq \tilde{\tilde{\mathbf{y}}}'_i}^{1 \leq i \leq N} \tilde{\tilde{\mathbf{o}}}'_i$
 - 12: **for** $k = 1, 2, \dots, M$ **do**
 - 13: Generate TEP e and calculate \mathcal{L}_e
 - 14: **if** $\mathcal{L}_e < \mathcal{L}_{thr}$ **then**
 - 15: Reencoding $\tilde{\tilde{\mathbf{c}}}_e = (\tilde{\tilde{\mathbf{y}}}' \oplus e) \cdot \tilde{\tilde{\mathbf{G}}}$
 - 16: Calculate WHD $D_e = \sum_{\tilde{\tilde{\mathbf{c}}}_e, i \neq \tilde{\tilde{\mathbf{y}}}'_i}^{1 \leq i \leq N} \tilde{\tilde{\mathbf{o}}}'_i$
 - 17: **if** $D_e \leq D_{opt}$ **then**
 - 18: $D_{opt} = D_e$, $\hat{\tilde{\tilde{\mathbf{c}}}} = \tilde{\tilde{\mathbf{c}}}_e$
 - 19: **end if**
 - 20: **end if**
 - 21: **end for**
 - 22: $\hat{\mathbf{y}}^i = \Pi_2^{-1}(\Pi_1^{-1}(\hat{\tilde{\tilde{\mathbf{c}}}}))$
 - 23: **end for**
 - 24: Obtain $\tilde{\mathbf{B}}_V = [\hat{\mathbf{y}}_{m+1:N}^1, \hat{\mathbf{y}}_{m+1:N}^2, \dots, \hat{\mathbf{y}}_{m+1:N}^{N-m}]^T$
 - 25: **end for**
 - 26: **return** $\tilde{\mathbf{B}}_1, \tilde{\mathbf{B}}_2, \dots$
-

and 1, estimated by the OSD algorithm, respectively. Obviously, either $\hat{\mathbf{c}}_{i=0}$ or $\hat{\mathbf{c}}_{i=1}$ is the optimal codeword estimation of the OSD algorithm.

In the SOSD-SWD algorithm, there are two types of decoding iterations. One is the SOSD decoding iteration for the component LDPC codes, referred to as the inner iteration with maximum iterations \mathcal{I} , and set $\mathcal{I} = 1$ for the sake of simplicity. The other is the number of iterations performed by SWD within a window, known as the outer iteration with maximum iterations \mathcal{J} .

The J -th outer iteration of target block \mathbf{B}_V in the SOSD-SWD structure is shown in Fig. 12, where the window size is $w = 4$. Let $\psi_t^{a,J}$ denote the a priori value of \mathbf{B}_t in the J th outer iteration, while $\psi_{t, re}^{a,J}$ corresponds to $\mathbf{B}_{t, re}$, and $\psi_t^{e,J}$ is the extrinsic information of \mathbf{B}_t obtained after the inner iteration in the J th outer iteration, while $\psi_{t, re}^{e,J}$ corresponds to $\mathbf{B}_{t, re}$.

The decoder of SOSD-SWD starts after $(w - 1)$ blocks are successfully received due to \mathbf{B}_0 is known. Without loss of generality, when decoding \mathbf{B}_V , there are w blocks are involved in the decoding process of SOSD-SWD algorithm, i.e., \mathbf{B}_t for $t \in [V - 1, V + w - 2]$ are participating the decoding of \mathbf{B}_V . Furthermore, there are three information

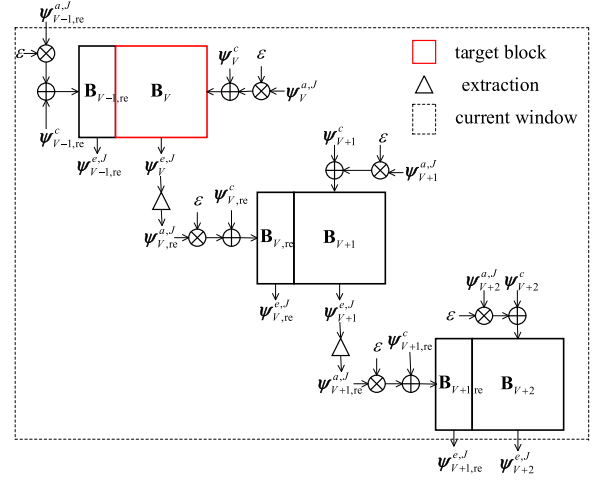


Fig. 12. SOSD-SWD process of the staircase LDPC codes with target block \mathbf{B}_V and $w = 4$.

Algorithm 2: SOSD-SWD Algorithm.

Input: $\psi_1^c, \psi_2^c, \dots, w, \mathcal{I}, \mathcal{J}, \varepsilon, m, \mathbf{G}, M$

Output: $\mathbf{B}_1, \mathbf{B}_2, \dots$

- 1: **for** $V = 1, 2, \dots$ **do**
 - 2: **if** $V=1$ **then**
 - 3: Initialize ψ_0^c as all zeros
 - 4: Initialize $\psi_0^{a,1}, \psi_1^{a,1}, \dots, \psi_{w-1}^{a,1}$ based on (44)
 - 5: **else**
 - 6: Obtain $\psi_{V-1}^{a,1}, \psi_V^{a,1}, \dots, \psi_{V+w-2}^{a,1}$ according to (43)
 - 7: **end if**
 - 8: **for** $j = 1, 2, \dots, \mathcal{J}$ **do**
 - 9: **for** $t = V, V + 1, \dots, V + w - 2$ **do**
 - 10: Obtain \mathbf{L}_t^c and $\mathbf{L}_t^{a,J}$
 - 11: Calculate $\mathbf{L}_V^{in,J} = \mathbf{L}_V^{c,J} + \varepsilon \cdot \mathbf{L}_V^{a,J}$
 - 12: **for** $c = 1, 2, \dots, N - m$ **do**
 - 13: Calculate $\mathbf{L}_{t,c}^{out,J}$ by $\mathbf{L}_{t,c}^{in,J}$ according to (42)
 - 14: **end for**
 - 15: Calculate $\mathbf{L}_V^{e,J} = \mathbf{L}_V^{out,J} - \mathbf{L}_V^{c,J}$
 - 16: Perform information exchange according to (45)
 - 17: **end for**
 - 18: Perform information exchange based on (46)
 - 19: **end for**
 - 20: Calculate $\tilde{\mathbf{B}}_V$ by hard-decision on $\mathbf{L}_V^{out,J}$
 - 21: **end for**
 - 22: **return** $\tilde{\mathbf{B}}_1, \tilde{\mathbf{B}}_2, \dots$
-

exchanges concerning the a priori values during the overall decoding process as follows.

The first information exchange occurs during the initialization process after the current window is determined

$$\psi_t^{a,1} = \begin{cases} \tilde{\psi}_t^{e,\mathcal{J}}, & t \in [V - 1, V + w - 3] \\ \mathbf{0}, & t = V + w - 2 \end{cases} \quad (43)$$

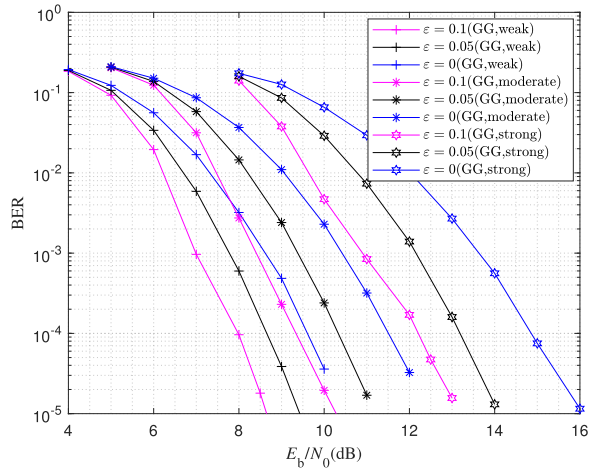


Fig. 13. Performance of SOSD-SWD at different ε with $N = 128$, $K = 64$, $m = 32$, $\mathcal{I} = 1$, $\mathcal{J} = 2$, and $M = 2$.

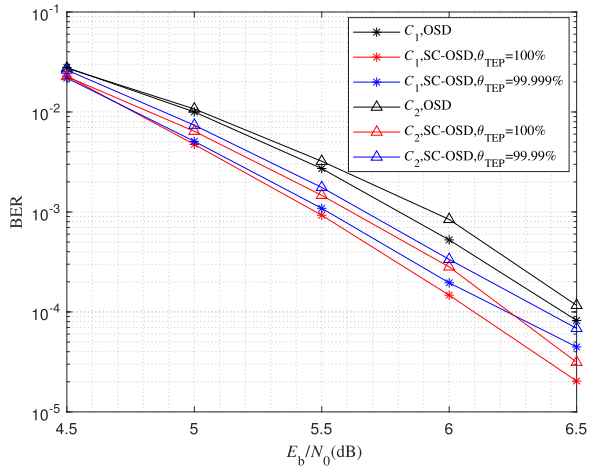


Fig. 14. BER Comparison of C_1 and C_2 under SC-OSD and OSD algorithms for BPPM in no scintillation state, where C_1 with $m = 12$, $\mu = 4$, $M = 3$ and C_2 with $m = 9$, $\mu = 4$, $M = 3$.

where $\bar{\psi}_t^{e,J}$ denotes the extrinsic information value of the t th block obtained after completing the last outer iteration during the decoding of \mathbf{B}_{V-1} , and $\mathbf{0}$ is an all-zero matrix. It is worth noting that when $V = 1$

$$\bar{\psi}_t^{a,1} = \mathbf{0}, t \in [0, w - 1]. \quad (44)$$

The second information exchange occurs between two adjacent blocks during one outer iteration process

$$\bar{\psi}_{t,\text{re}}^{a,J} = \bar{\psi}_{t,\text{re}}^{e,J}, t \in [V, V + w - 3]. \quad (45)$$

The third information exchange occurs between two consecutive outer iteration processes, specifically at the beginning of the J th outer iteration process, where $1 < J \leq \mathcal{J}$

$$\bar{\psi}_{t,\text{re}}^{a,J} = \bar{\psi}_{t,\text{re}}^{e,J-1}, t = V - 1 \quad (46a)$$

$$\bar{\psi}_t^{a,J} = \bar{\psi}_t^{e,J-1}, t \in [V, V + w - 2]. \quad (46b)$$

During the J th outer iteration, the input LLR matrix for the SOSD is denoted as $\mathbf{L}_V^{\text{in},J}$ when

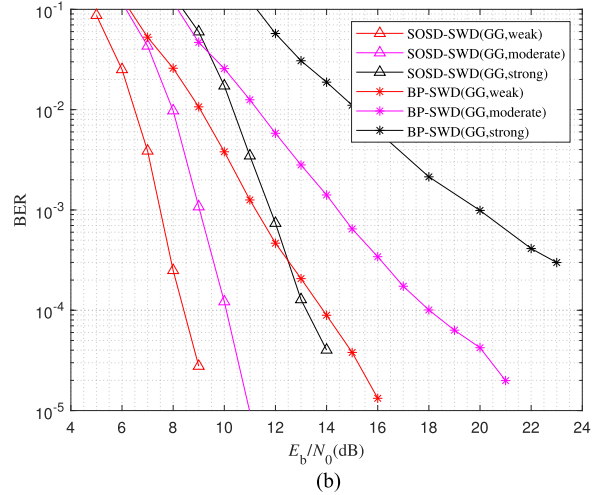
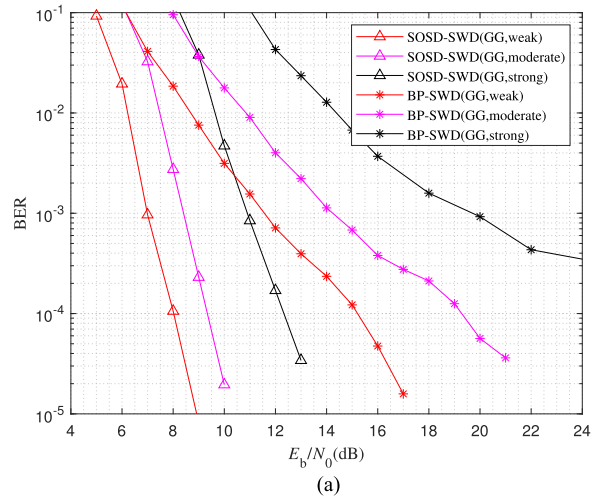


Fig. 15. BER comparison of C_1 and C_2 under SOSD-SWD and BP-SWD algorithms for 4PPM in different turbulence conditions. (a) Comparison BER of C_1 under SOSD-SWD algorithm with $\mathcal{I} = 1$, $\mathcal{J} = 2$, and $M = 2$ and BP-SWD algorithm with $\mathcal{I} = 10$, and $\mathcal{J} = 20$ for 4PPM with $m = 32$, $w = 4$, and $\varepsilon = 0.1$. (b) Comparison of BER of C_2 under SOSD-SWD algorithm with $\mathcal{I} = 1$, $\mathcal{J} = 2$, and $M = 2$ and BP-SWD algorithm with $\mathcal{I} = 10$, and $\mathcal{J} = 20$ for 4PPM with $m = 24$, $w = 4$, and $\varepsilon = 0.1$.

decoding $[\mathbf{B}_{V-1,\text{re}}, \mathbf{B}_V]$, $\mathbf{L}_V^{\text{in},J} = \mathbf{L}_V^{c,J} + \varepsilon \cdot \mathbf{L}_V^{a,J}$, where $\mathbf{L}_V^{a,J} = [\psi_{V-1,\text{re}}^{a,J}, \psi_V^{a,J}]$, $\mathbf{L}_V^{c,J} = [\psi_{V-1,\text{re}}^{c,J}, \psi_V^{c,J}]$, and ε is a scaling factor. Using the parallel SOSD, $\mathbf{L}_V^{\text{in},J} = [l_{V,1}^{\text{in},J}, l_{V,2}^{\text{in},J}, \dots, l_{V,N-m}^{\text{in},J}]^T$ is processed row-wise, and we can obtain the corresponding output LLR matrix $\mathbf{L}_V^{\text{out},J} = [l_{V,1}^{\text{out},J}, l_{V,2}^{\text{out},J}, \dots, l_{V,N-m}^{\text{out},J}]^T$. Then, we can obtain $\mathbf{L}_V^{e,J} = \mathbf{L}_V^{\text{out},J} - \mathbf{L}_V^{c,J}$ where $\mathbf{L}_V^{e,J} = [\psi_{V-1,\text{re}}^{e,J}, \psi_V^{e,J}]$.

The outer iteration process is repeated until $J = \mathcal{J}$ is completed, and the decoder outputs the estimated values $\tilde{\mathbf{B}}_V$ of the target block \mathbf{B}_V . In the subsequent decoding of the next target block \mathbf{B}_{V+1} , the decoder receives a new block \mathbf{B}_{V+w} , and the decoding window slides one block, at which point the current window includes blocks $\mathbf{B}_V, \mathbf{B}_{V+1}, \dots, \mathbf{B}_{V+w-1}$. The entire decoding process of SOSD-SWD is repeated continuously.

In conclusion, the extrinsic information values are obtained using the doubly iteration process, and then are used

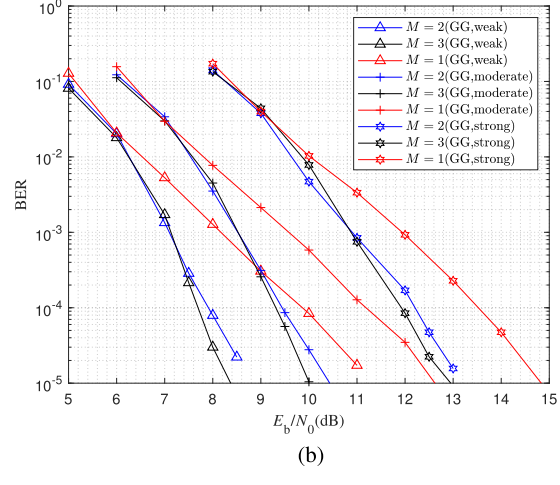
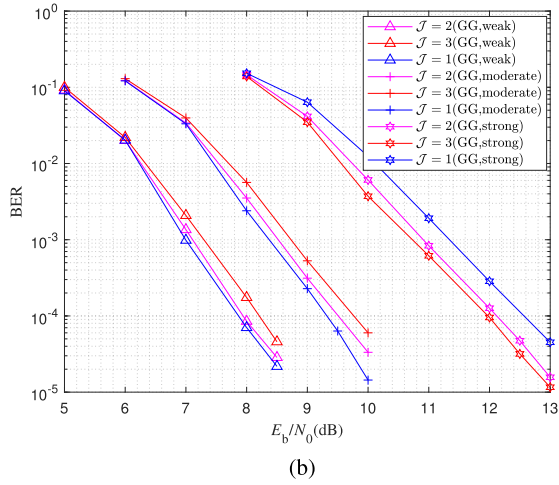
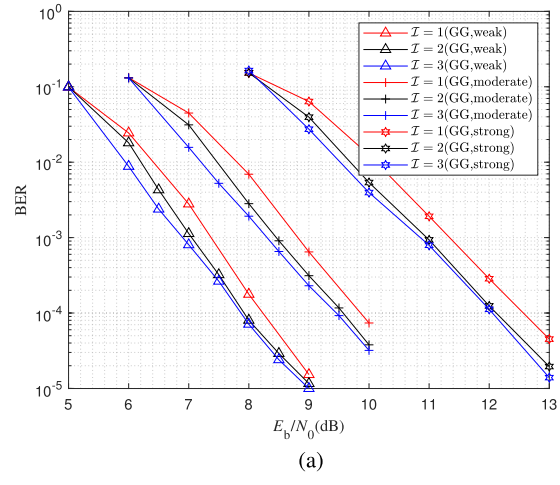
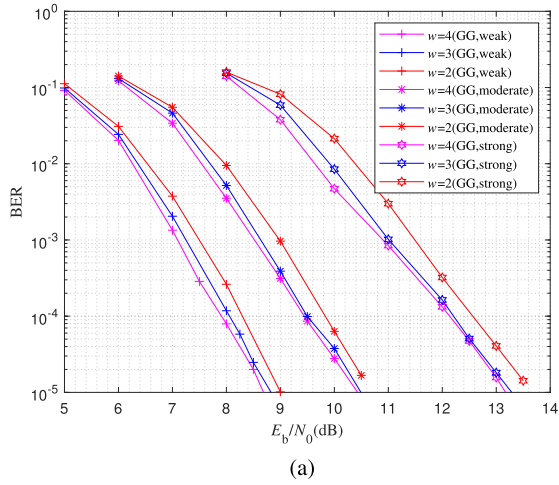


Fig. 16. Performance of SOSD-SWD at different SWD parameters. (a) Performance of SOSD-SWD at different w . (b) The performance of SOSD-SWD at different \mathcal{J} .

Fig. 17. Performance of SOSD-SWD at different S OSD parameters. (a) Performance of SOSD-SWD scheme at different \mathcal{I} . (b) The performance of SOSD-SWD scheme at different M .

as a prior values for subsequent decoding in the SOSD-SWD algorithm. The input LLR of the S OSD, which is used for component LDPC codes, consists of the intrinsic values and the a prior values. This operation changes the reliability of the original input sequence and even changes the composition of the original MRB and LRB. As a result, the errors with lower reliability values may be corrected before the reencoding operation. The errors with higher reliability values may lower their LLRs, which can be more easily corrected during the subsequent reencoding operation. The SOSD-SWD algorithm is summarized in Algorithm 2. Fig. 13 provides evidence for the rationale of our proposed SOSD-SWD, where $\varepsilon = 0$ represents the worst performance scenario, i.e., not utilizing the iterative soft information in SWD, which is proved that this structure can significantly improve decoding performance.

IV. SIMULATION RESULTS

In this section, we first evaluate the performance of SC-OSD and SOSD-SWD for staircase LDPC codes under the synodic period channel. Then, we discuss the number of reencoding operations of SC-OSD. Finally, we investigate

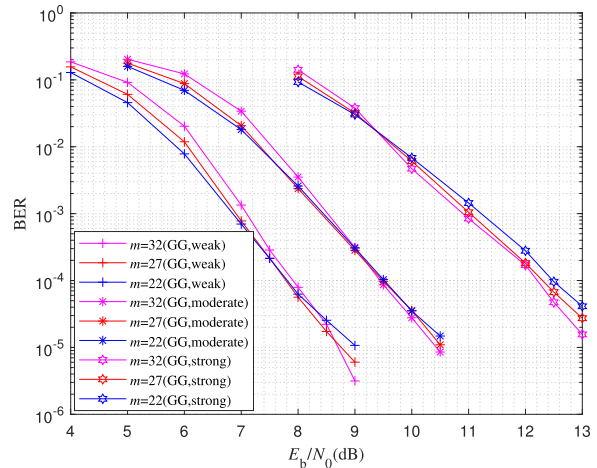


Fig. 18. Performance of SOSD-SWD at different m .

the impact of various parameters on the SOSD-SWD by Monte Carlo simulations. The first component LDPC code C_1 in our simulation is from [45] with parameters $N = 128$ and $K = 64$, and the second component LDPC code C_2 is from [46] with parameters $N = 96$ and $K = 48$.

TABLE III
Compare the Number of Reencoding Operations With $M = 3$

E_b/N_0 (dB)	4.5	5	5.5	6	6.5
OSD	43745	43745	43745	43745	43745
SC-OSD	30553	27834	24401	19360	13737

Fig. 14 illustrates the BER comparison of C_1 and C_2 under SC-OSD and OSD algorithms in no scintillation state, and Fig. 15 shows the BER comparison of C_1 and C_2 under S OSD-SWD and BP-SWD algorithms with different turbulence conditions, respectively. It can be seen that with the increase in turbulence intensity, the improvement of S OSD-SWD is more significant compared to BP-OSD. Moreover, the BER of C_1 outperforms that of C_2 in various parameters, and we utilize C_1 in the following simulations.

Table III compares the number of reencoding operation between SC-OSD with $\theta_{\text{TEP}} = 99.999\%$ and OSD for C_1 , we can find that the SC-OSD can reduce half of the complexity of reprocessing the TEP with an increase in SNR.

The performance of S OSD-SWD in relation to the parameters of SWD and S OSD are shown in Figs. 16 and 17, respectively. Increasing the window size means that more staircase blocks participate in the decoding process of the target block, which can improve the performance of S OSD-SWD. Within a fixed sliding window, each complete codeword in the target staircase block undergoes a total of $(\mathcal{I} \cdot \mathcal{J})$ S OSD decoding iterations. Therefore, increasing either \mathcal{I} or \mathcal{J} can ensure lower BER. Moreover, Fig. 17(b) shows that the increasing of M leads to lower BER at high SNR, but it also increases complexity significantly due to the increase in the number of reencoding operations.

Fig. 18 illustrates that a higher SNR can improve decoding performance with more reencoded bits at the encoder side, resulting in more reliable transmission. The higher the solar scintillation, the more significant the improvement in decoding performance.

V. CONCLUSION

In this article, we proposed the SC-OSD algorithm and the S OSD-SWD algorithm for deep space optical communications. We first divided the channel states based on the threshold of $\sigma_I^2 = 0.01$ and $\sigma_I^2 = 0.99$, within the synodic period of 780 days between Mars–Earth. Then, we modified the traditional OSD for the staircase LDPC codes to design the SC-OSD algorithm, and the proposed skip criterion can reduce the reencoding operations by approximately 50% at $E_b/N_0 = 6$ dB. Moreover, we utilized the S OSD as the inner decoder to design the S OSD-SWD algorithm under a scintillation state. Under the strong scintillation, our S OSD-SWD can overcome the error floor compared to BP-SWD, and can provide approximately 30 dB performance gain over the uncoded system for 10^{-4} BER. Finally, simulation results showed that the increasing of w , \mathcal{I} , \mathcal{J} , and M can improve S OSD-SWD performance at the cost of complexity, which can be carefully considered in our future work.

APPENDIX A DERIVATION OF $\mathbb{E}[\tilde{\sigma}_u]$ AND $\sigma_{\tilde{\sigma}_u}^2$

We define the following random variables:

$$v_N^m = \sum_{v=1}^{N-m} \mathbf{1}_{[0,t]}(o_v) + \sum_{v=1}^m \mathbf{1}_{[0,t]}(o'_v)$$

it can be noted that for any $t > 0$, there exists an equivalence relation $\{\tilde{\sigma}_u \geq t\} \equiv \{v_N^m \leq N - u\}$, where $\mathbf{1}_{\mathcal{X}}(x) = 1$ if $x \in \mathcal{X}$ and $\mathbf{1}_{\mathcal{X}}(x) = 0$, otherwise. v_n is composed of two binomial distributions, $\mathcal{B}(N - m, F_o(t))$ and $\mathcal{B}(m, F_o'(t))$, and according to the Demoivre–Laplace theorem, it can be approximated as a normal distribution with mean

$$\mathbb{E}[v_N^m] = (N - m)F_o(t) + mF_o'(t)$$

and variance

$$\sigma_{v_N^m}^2 = (N - m)F_o(t)(1 - F_o(t)) + mF_o'(t)(1 - F_o'(t)).$$

Then, we define a random variable dependent on t as

$$g(t) = \frac{t(N - v_N^m)}{u}$$

obviously $g(t)$ is also a normal random variable, and the following equivalence relationship exists:

$$\begin{aligned} \{\tilde{\sigma}_u \geq t\} &\equiv \{g(t) \geq t\} \\ &\equiv \left\{ \mathcal{N} \left(\frac{t(N - \mathbb{E}[v_N^m])}{u}, \frac{t^2 \sigma_{v_N^m}^2}{u^2} \right) \geq t \right\}. \end{aligned}$$

Assuming that $\tilde{\sigma}_u$ follows a normal distribution $\mathcal{N}(\mathbb{E}[\tilde{\sigma}_u], \sigma_{\tilde{\sigma}_u}^2)$, its mean and variance should be independent of t , and we have

$$\begin{aligned} \Pr \left(\mathcal{N} \left(\mathbb{E}[\tilde{\sigma}_u], \sigma_{\tilde{\sigma}_u}^2 \right) \geq t \right) \\ = \Pr \left(\mathcal{N} \left(\frac{t(N - \mathbb{E}[v_N^m])}{u}, \frac{t^2 \sigma_{v_N^m}^2}{u^2} \right) \geq t \right). \end{aligned}$$

Let $t = t' = \mathbb{E}[\tilde{\sigma}_u]$, we can obtain that

$$\begin{aligned} \Pr \left(\mathcal{N} \left(\mathbb{E}[\tilde{\sigma}_u], \sigma_{\tilde{\sigma}_u}^2 \right) \geq \mathbb{E}[\tilde{\sigma}_u] \right) \\ = \Pr \left(\mathcal{N} \left(\frac{\mathbb{E}[\tilde{\sigma}_u](N - \mathbb{E}[v_N^m])}{u}, \frac{(\mathbb{E}[\tilde{\sigma}_u])^2 \sigma_{v_N^m}^2}{u^2} \right) \geq \mathbb{E}[\tilde{\sigma}_u] \right) \\ = \frac{1}{2} \end{aligned}$$

and

$$\frac{\mathbb{E}[\tilde{\sigma}_u](N - \mathbb{E}[v_N^m])}{u} = \mathbb{E}[\tilde{\sigma}_u].$$

Therefore

$$\left(\frac{N - m}{N - u} \right) F_o(\mathbb{E}[\tilde{\sigma}_u]) + \left(\frac{m}{N - u} \right) F_o'(\mathbb{E}[\tilde{\sigma}_u]) = 1$$

since $F_o(x)$ and $F_o'(x)$ are monotonically increasing functions, there exists only one $\mathbb{E}[\tilde{\sigma}_u]$ that satisfies the above equation.

We can also obtain that

$$\begin{aligned} \{\tilde{\sigma}_u \geq t\} &\equiv \left\{ \mathcal{N}(0, 1) \geq \frac{u - N + \mathbb{E}[v_N^m]}{\sqrt{\sigma_{v_N^m}^2}} \right\} \\ &\equiv \left\{ \mathcal{N}(0, 1) \geq -\frac{u - N + \mathbb{E}[v_N^m]}{(t - t')\sqrt{\sigma_{v_N^m}^2}} t' \right. \\ &\quad \left. + \frac{u - N + \mathbb{E}[v_N^m]}{(t - t')\sqrt{\sigma_{v_N^m}^2}} t \right\}. \end{aligned}$$

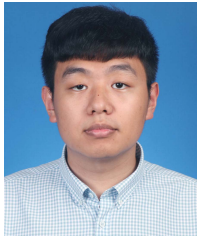
From above, the variance is given by

$$\begin{aligned} \sigma_{\tilde{\sigma}_u}^2 &= \lim_{t \rightarrow t'} \frac{(t - t')^2 \sigma_{v_N^m}^2}{(u - N + \mathbb{E}[v_N^m])^2} \\ &= \frac{N - u - (N - m)F_o(\mathbb{E}[\tilde{\sigma}_u])^2 - mF_{\sigma'}(\mathbb{E}[\tilde{\sigma}_u])^2}{((N - m)f_o(\mathbb{E}[\tilde{\sigma}_u]) + mf_{\sigma'}(\mathbb{E}[\tilde{\sigma}_u])^2)}. \end{aligned}$$

REFERENCES

- [1] J. Taylor, *Deep Space Communications*. Hoboken, NJ, USA: Wiley, 2016.
- [2] S. Wu et al., "CS-LTP-Spinal: A cross-layer optimized rate-adaptive image transmission system for deep-space exploration," *Sci. China Inf. Sci.*, vol. 65, 2022, Art. no. 112303.
- [3] A. S. Hamza, J. S. Deogun, and D. R. Alexander, "Classification framework for free space optical communication links and systems," *IEEE Commun. Surv. Tuts.*, vol. 21, no. 2, pp. 1346–1382, Secondquarter 2019.
- [4] H. Kaushal and G. Kaddoum, "Optical communication in space: Challenges and mitigation techniques," *IEEE Commun. Surv. Tuts.*, vol. 19, no. 1, pp. 57–96, Firstquarter 2017.
- [5] M. S. Bashir, "Free-space optical communications with detector arrays: A mathematical analysis," *IEEE Trans. Aerosp. Electron. Syst.*, vol. 56, no. 2, pp. 1420–1429, Apr. 2020.
- [6] M. A. Khalighi and M. Uysal, "Survey on free space optical communication: A communication theory perspective," *IEEE Commun. Surv. Tuts.*, vol. 16, no. 4, pp. 2231–2258, Fourthquarter 2014.
- [7] D. J. Costello and G. D. Forney, "Channel coding: The road to channel capacity," *Proc. IEEE*, vol. 95, no. 6, pp. 1150–1177, Jun. 2007.
- [8] B. Epplé, "Simplified channel model for simulation of free-space optical communications," *J. Opt. Commun. Netw.*, vol. 2, no. 5, pp. 293–304, May 2010.
- [9] H. Ivanov, E. Leitgeb, and G. Freiberger, "Characterization of poisson channel for deep space FSO based on SNSPD technology by experimental demonstration," in *Proc. 11th Int. Symp. Commun. Syst., Netw. Digit. Signal Process.*, 2018, pp. 1–5.
- [10] A. J. Hashmi, A. Eftikhar, A. Adibi, and F. Amoozegar, "Optimization of an optical array receiver for deep-space optical communication during Earth-Mars conjunction phase," in *Proc. Photon. Glob. Conf.*, 2012, pp. 1–5.
- [11] G. Xu and Z. Song, "Effects of solar scintillation on deep space communications: Challenges and prediction techniques," *IEEE Wireless Commun.*, vol. 26, no. 2, pp. 10–16, Apr. 2019.
- [12] G. Xu and Q. Zhang, "Mixed RF/FSO deep space communication system under solar scintillation effect," *IEEE Trans. Aerosp. Electron. Syst.*, vol. 57, no. 5, pp. 3237–3251, Oct. 2021.
- [13] G. Xu and M. Zeng, "Solar scintillation effect for optical waves propagating through gamma-gamma coronal turbulence channels," *IEEE Photon. J.*, vol. 11, no. 4, 2019, Art. no. 7904415.
- [14] C. Condo and G. Masera, "Unified turbo/LDPC code decoder architecture for deep-space communications," *IEEE Trans. Aerosp. Electron. Syst.*, vol. 50, no. 4, pp. 3115–3125, Oct. 2014.
- [15] B. P. Smith, A. Farhood, A. Hunt, F. R. Kschischang, and J. Lodge, "Staircase codes: FEC for 100 Gb/s OTN," *J. Lightw. Technol.*, vol. 30, no. 1, pp. 110–117, Jan. 2012.
- [16] X. Dou, M. Zhu, J. Zhang, and B. Bai, "Soft-decision based sliding-window decoding of staircase codes," in *Proc. IEEE 10th Int. Symp. Turbo Codes Iterative Inf. Process.*, 2018, pp. 1–5.
- [17] A. Sheikh, A. G. i Amat, and A. Alvarado, "Novel high-throughput decoding algorithms for product and staircase codes based on error-and-erasure decoding," *J. Lightw. Technol.*, vol. 39, no. 15, pp. 4909–4922, Aug. 2021.
- [18] T. Mehmood, M. P. Yankov, S. Iqbal, and S. Forchhammer, "Flexible multilevel coding with concatenated polar-staircase codes for M-QAM," *IEEE Trans. Commun.*, vol. 69, no. 2, pp. 728–739, Feb. 2021.
- [19] Y. Zhang and I. B. Djordjevic, "Staircase rate-adaptive LDPC-coded modulation for high-speed intelligent optical transmission," in *Proc. IEEE Opt. Fiber Commun.*, 2014, pp. 1–3.
- [20] V. B. Wijekoon, E. Viterbo, and Y. Hong, "LDPC-staircase codes for soft decision decoding," in *Proc. IEEE Wireless Commun. Netw. Conf.*, 2020, pp. 1–6.
- [21] L. M. Zhang and F. R. Kschischang, "Complexity-optimized concatenated LDGM-staircase codes," in *Proc. IEEE Int. Symp. Inf. Theory*, 2017, pp. 1688–1692.
- [22] L. M. Zhang and F. R. Kschischang, "Low-complexity soft-decision concatenated LDGM-staircase FEC for high-bit-rate fiber-optic communication," *J. Lightw. Technol.*, vol. 35, no. 18, pp. 3991–3999, Sep. 2017.
- [23] M. Barakatain and F. R. Kschischang, "Low-complexity concatenated LDPC-staircase codes," *J. Lightw. Technol.*, vol. 36, no. 12, pp. 2443–2449, Jun. 2018.
- [24] L. Holzbaur, H. Bartz, and A. Wachter-Zeh, "Improved decoding and error floor analysis of staircase codes," *Des., Codes Cryptogr.*, vol. 87, pp. 647–664, 2019.
- [25] R. Jose and A. Pe, "Analysis of hard decision and soft decision decoding algorithms of LDPC codes in AWGN," in *Proc. IEEE Int. Adv. Comput. Conf.*, 2015, pp. 430–435.
- [26] M. P. Fossorier and S. Lin, "Soft-decision decoding of linear block codes based on ordered statistics," *IEEE Trans. Inf. Theory*, vol. 41, no. 5, pp. 1379–1396, Sep. 1995.
- [27] Y. Wu and C. N. Hadjicostis, "Soft-decision decoding using ordered recodings on the most reliable basis," *IEEE Trans. Inf. Theory*, vol. 53, no. 2, pp. 829–836, Feb. 2007.
- [28] W. Jin and M. Fossorier, "Probabilistic sufficient conditions on optimality for reliability based decoding of linear block codes," in *Proc. IEEE Int. Symp. Inf. Theory*, 2006, pp. 2235–2239.
- [29] F. Wang, J. Jiao, K. Zhang, S. Wu, and Q. Zhang, "Adjustable ordered statistic decoder for short block length code towards URLLC," in *Proc. 13th Int. Conf. Wireless Commun. Signal Process.*, 2021, pp. 1–5.
- [30] C. Yue, M. Shirvanimoghaddam, B. Vucetic, and Y. Li, "A revisit to ordered statistics decoding: Distance distribution and decoding rules," *IEEE Trans. Inf. Theory*, vol. 67, no. 7, pp. 4288–4337, Jul. 2021.
- [31] M. P. Fossorier and S. Lin, "Soft-input soft-output decoding of linear block codes based on ordered statistics," in *Proc. IEEE GLOBECOM*, 1998, pp. 2828–2833.
- [32] C. Yue et al., "NOMA joint decoding based on soft-output ordered-statistics decoder for short block codes," in *ICC 2022-IEEE Int. Conf. Commun.*, 2022, pp. 2163–2168.
- [33] M. Al-Habash, L. C. Andrews, and R. L. Phillips, "Mathematical model for the irradiance probability density function of a laser beam propagating through turbulent media," *Opt. Eng.*, vol. 40, no. 8, pp. 1554–1562, 2001.
- [34] G. Xu and M. Zeng, "Solar scintillation effect for optical waves propagating through gamma-gamma coronal turbulence channels," *IEEE Photon. J.*, vol. 11, no. 4, Aug. 2019, Art. no. 7904415.
- [35] G. Xu, Z. Zheng, and W. Wang, "Dual-hop deep space-terrestrial FSO/RF communication under solar scintillation: Performance analysis and challenges," *China Commun.*, vol. 17, no. 7, pp. 27–37, 2020.

- [36] C. M. Ho, M. K. Sue, A. Bedrossian, and R. Sniffin, "Scintillation effects on radio wave propagation through solar Corona," 2002. [Online]. Available: <https://ntrs.nasa.gov/search.jsp?R=20060029492>
- [37] A. E. Abouelez, "Performance analysis of an L-ary PPM MISO ground-to-satellite free-space laser link with an APD-based receiver over a Málaga turbulence channel in the presence of beam wander," *J. Opt. Commun. Netw.*, vol. 14, no. 3, pp. 100–110, 2022.
- [38] M. S. Bashir and S. S. Muhammad, "Time synchronization in photon-limited deep space optical communications," *IEEE Trans. Aerosp. Electron. Syst.*, vol. 56, no. 1, pp. 30–40, Feb. 2020.
- [39] "Wolfram," 2023. [Online]. Available: <https://functions.wolfram.com/>
- [40] A. Kabat, F. Guilloud, and R. Pyndiah, "New approach to order statistics decoding of long linear block codes," in *Proc. IEEE Glob. Telecommun. Conf.*, 2007, pp. 1467–1471.
- [41] J. Van Wouwerghem, A. Alloum, J. J. Boutros, and M. Moeneclaey, "On short-length error-correcting codes for 5G-NR," *Ad Hoc Netw.*, vol. 79, pp. 53–62, 2018.
- [42] F. Wang et al., "Self-adaptive ordered statistics decoder for finite block length raptor codes toward URLLC," *IEEE Internet Things J.*, vol. 9, no. 5, pp. 3282–3297, Mar. 2022.
- [43] F. Wang et al., "Efficient ordered statistics decoder for ultra-reliable low latency communications," in *Proc. IEEE Int. Conf. Commun.*, Montreal, Canada, 2021, pp. 1–6.
- [44] C. Yue et al., "NOMA joint decoding based on soft-output ordered-statistics decoder for short block codes," in *Proc. IEEE Int. Conf. Commun.*, 2022, pp. 2163–2168.
- [45] M. Helmling et al., "Database of channel codes and ML simulation results," 2019. [Online]. Available: www.uni-kl.de/channel-codes
- [46] C. Poulliat, M. Fossorier, and D. Declercq, "Design of regular (2,d/sub c)-LDPC codes over GF(q) using their binary images," *IEEE Trans. Commun.*, vol. 56, no. 10, pp. 1626–1635, Oct. 2008.



Yaosheng Zhang (Graduate Student Member, IEEE) received the B.E. degree in information engineering from Shandong University, Qingdao, China, in 2021, and the masters degree in electronics and communication engineering from the Harbin Institute of Technology (Shenzhen), Shenzhen, China, in 2023, where he is currently pursuing the Ph.D. degree in information and communication engineering with the Guangdong Provincial Key Laboratory of Aerospace Communication and Networking Technology.

His research interests include error control coding, channel modeling, satellite communications and free space optical communications.



Jian Jiao (Senior Member, IEEE) received the M.S. and Ph.D. degrees in communication engineering from the Harbin Institute of Technology (HIT), Harbin, China, in 2007 and 2011, respectively.

From 2011 to 2015, he was a Post-Doctoral Research Fellow at the Communication Engineering Research Centre, Harbin Institute of Technology Shenzhen Graduate School, Shenzhen, China. From 2016 to 2017, he was a China Scholarship Council Visiting Scholar at

the School of Electrical and Information Engineering, The University of Sydney, Sydney, Australia. From 2017, he was at the Harbin Institute of Technology Shenzhen (HITSz), where he has been a Professor with the Guangdong Provincial Key Laboratory of Aerospace Communication and Networking Technology, since 2022. He is also an Associate Professor with Peng Cheng Laboratory, Shenzhen. He is currently serving as an Editor for Science China Information Sciences. His current interests include semantic communications, satellite communications and networking, and coding techniques.

Dr. Jiao is currently serving as an Editor for *Science China Information Sciences*.



Ke Zhang (Member, IEEE) received the master's degree in information and communication engineering from the Harbin Institute of Technology, Shenzhen, China, in 2017, and the Ph.D. degree in information and communication engineering from the Harbin Institute of Technology, Harbin, China, in 2022.

He is currently a Postdoctoral Research Fellow with the Peng Cheng Laboratory, Shenzhen, China. His research interests include short block-length channel codes and decoder and satellite communications.



Ye Wang (Member, IEEE) received his M.S. and Ph.D. degrees in information and communication engineering from Harbin Institute of Technology (HIT), Harbin, China, in 2009 and 2013, respectively.

From 2013 to 2014, he was a Post-Doctoral Research Fellow with the University of Ontario Institute of Technology, Canada. From 2015 to 2021, he was an Assistant Professor with the Harbin Institute of Technology Shenzhen (HITSz). Since 2022, he has been an Associate

Professor with Peng Cheng Laboratory, Shenzhen. His research interests include satellite communications, resource allocation, and mobile internet.



Rongxing Lu (Fellow, IEEE) received the Ph.D. degree from the Department of Electrical and Computer Engineering, University of Waterloo, Canada, in 2012.

He is a Mastercard IoT Research Chair, a University Research Scholar, an associate professor at the Faculty of Computer Science (FCS), University of New Brunswick (UNB), Canada. Before that, he worked as an assistant professor at the School of Electrical and Electronic Engineering, Nanyang Technological University

(NTU), Singapore from 2013 to 2016. Rongxing Lu worked as a Postdoctoral Fellow at the University of Waterloo from 2012 to 2013.

He was awarded the most prestigious "Governor General's Gold Medal," when he received his PhD degree from the Department of Electrical and Computer Engineering, University of Waterloo, Canada, in 2012; and won the 8th IEEE Communications Society (ComSoc) Asia Pacific (AP) Outstanding Young Researcher Award, in 2013. Dr. Lu is an IEEE Fellow. His research interests include applied cryptography, privacy enhancing technologies, and IoT-Big Data security and privacy. He has published extensively in his areas of expertise, and was the recipient of nine best (student) paper awards from some reputable journals and conferences. Currently, Dr. Lu serves as the Chair of IEEE ComSoc CIS-TC (Communications and Information Security Technical Committee), and the founding Co-chair of IEEE TEMS Blockchain and Distributed Ledgers Technologies Technical Committee (BDLT-TC). Dr. Lu is the Winner of 2016–2017 Excellence in Teaching Award, FCS, UNB.



Qinyu Zhang (Senior Member, IEEE) received the bachelors degree in communication engineering from the Harbin Institute of Technology (HIT) in 1994 and the Ph.D. degree in biomedical and electrical engineering from the University of Tokushima, Japan, in 2003.

From 1999 to 2003, he was an Assistant Professor with the University of Tokushima. He has been with Harbin Institute of Technology-Shenzhen (HITSz) since 2003, he is currently a full professor and and serves as the Vice

President of HITSz.

He has been awarded the National Science Fund for Distinguished Young Scholars, Young and Middle-aged Leading Scientist of China, the Chinese New Century Excellent Talents in University, etc., and obtained three scientific and technological awards from governments.

His research interests include aerospace communications and networks, wireless communications and networks.